FeOOH and (Fe,Zn)OOH hybrid anion exchange adsorbents for phosphate recovery
A determination of Fe-phases and adsorption–desorption mechanisms

Belloni, C.; Korving, L.; Witkamp, G. J.; Brück, E.; de Jager, P.; Dugulan, A. I.

DOI
10.1016/j.cej.2023.145287

Publication date
2023

Document Version
Final published version

Published in
Chemical Engineering Journal

Citation (APA)
Belloni, C., Korving, L., Witkamp, G. J., Brück, E., de Jager, P., & Dugulan, A. I. (2023). FeOOH and (Fe,Zn)OOH hybrid anion exchange adsorbents for phosphate recovery: A determination of Fe-phases and adsorption–desorption mechanisms. *Chemical Engineering Journal*, *473*, Article 145287. https://doi.org/10.1016/j.cej.2023.145287

Chemical Engineering Journal 473 (2023) 145287

Contents lists available at ScienceDirect

Chemical Engineering Journal

journal homepage: www.elsevier.com/locate/cej

FeOOH and (Fe,Zn)OOH hybrid anion exchange adsorbents for phosphate recovery: A determination of Fe-phases and adsorption–desorption mechanisms

C. Belloni [a,b,*], L. Korving [a], G.J. Witkamp [c], E. Brück [b], P. de Jager [d], A.I. Dugulan [b]

[a] Wetsus, European Centre of Excellence for Sustainable Water Technology, Oostergoweg 9, 8911 MA Leeuwarden, the Netherlands
[b] Fundamental Aspects Mat & Energy Group, Delft University of Technology, Mekelweg 15, 2629 JB Delft, the Netherlands
[c] Water Desalination and Reuse Center, Biological and Environmental Science and Engineering Division, King Abdullah University of Science and Technology, Saudi Arabia
[d] Aquacare Europe BV, Graaf van Solmsweg 56-58, 5222 BP 's-Hertogensbosch, the Netherlands

ARTICLE INFO

Keywords:
Phosphate adsorption
Hybrid anion exchange adsorbents
Iron oxide doping
Adsorbent regeneration
Water treatment
Resource recovery

ABSTRACT

Hybrid anion exchange adsorbents (HAIX) seem promising to prevent eutrophication and recover phosphate (P). HAIX consist of an anion exchange resin (AIX) backbone, promoting anion physisorption (outer-sphere complex), impregnated with iron (hydr)oxide nanoparticles (NPs), for selective P chemisorption (inner-sphere complex). In this work, for the first time, as far as we know, Zn-doped iron (hydr)oxide NPs were embedded in AIX, and the performances compared with conventional HAIX, both commercial and synthesized. Zn-doped HAIX displayed improved P adsorption performances. Mössbauer spectroscopy (MS) revealed the goethite nature of the NPs, against the "amorphous hydrous ferric oxide" claimed in literature. The P adsorption comparisons, made in synthetic solution and real wastewater, underlined the crucial role of the NPs for selective P adsorption, while improving the understanding on the competition between physisorption and chemisorption. In pure P synthetic solutions, especially at high P concentrations, physisorption can "hide" chemisorption. This depends also on the anion form of the AIX, due to their higher affinity for multivalent anions, which affects HAIX adsorption selectivity and P desorption. In fact, a mild alkaline regeneration over three adsorption–desorption cycles revealed a complex interaction between the regenerant OH^- and the adsorbed P. OH^- molecules are consumed to transform phosphate speciation, causing (stronger) P re-adsorption and preventing desorption. Finally, Mössbauer spectroscopy revealed NPs agglomeration/growth after the three cycles plus final regeneration at pH 14. This study provides further understanding on the P adsorption–desorption mechanism in HAIX, drawing attention on the choice of experimental conditions for reliable performance assessment, and questioning HAIX consistent P removal and efficient P recovery in the long-term.

1. Introduction

Hybrid anion exchanger adsorbents (HAIX), widely applied for arsenic (As) removal [1–5], showed promising results for phosphate (P) recovery [6–9]. HAIX displayed potential to reach ultra-low P concentrations [10,11], necessary to prevent eutrophication [12]. HAIX consist of an anion exchange resin (AIX) backbone impregnated with metal (hydr)oxide nanoparticles (NPs) often iron oxides (comprising hydroxide and oxyhydroxides) [7–9,13], displaying a twofold adsorption mechanism. Firstly, the resin backbone, which provides the Donnan exclusion effect [14–16], promotes anion physisorption, which is charge driven (either via electrostatic, hydrogen bond, or outer-sphere complexation), hence with little selectivity among different anionic species. The anionic interaction and adsorption mechanism depend on the backbone material, the adsorption sites and their anion form (positively charged site loaded with an anion), usually sulfate or chloride [13,17–19]. Secondly, the NPs, which according to previous studies [4,9,16,20] provide higher selectivity, binding phosphate via chemisorption, in the sense that they form a chemical bond via inner-sphere complexation. The NPs role is fundamental for treating complex water matrices for phosphate (henceforth referred to as P) recovery. Iron oxides show good affinity for P, are abundant and relatively cheap

* Corresponding author.
E-mail address: carlo.belloni@wetsus.nl (C. Belloni).

https://doi.org/10.1016/j.cej.2023.145287
Received 4 August 2023; Accepted 6 August 2023
Available online 9 August 2023

compounds, and have been widely investigated [6,10,20–24]. Different HAIX synthesis methods are available in literature [5,25–27] and commercial adsorbents, like Layne^{RT}, have been widely investigated [4,7–9,13,25,28]. These, and in particular Layne^{RT}, are usually claimed to contain amorphous/non-crystalline iron oxide nanoparticles, defined with the general and non-specific term "hydrous ferric oxide", HFO, mostly ascribed to ferrihydrite [3,4,6–9,11,26,29–36]. These claims are either based on TEM and XRD observations, or on previous research (where TEM and XRD were employed). However, both techniques show limitations when dealing with ultrafine NPs (<15–20 nm). This paper aims to provide a finer characterization by means of Mössbauer spectroscopy, which is able to better identify iron oxide phases down to lower NP sizes, and also able to work with amorphous compounds. Table 1.

For the economic viability of adsorption technology for P recovery, it is necessary to be able to regenerate and reuse the adsorbent for multiple adsorption cycles [10]. This is typically performed with an alkaline wash, e.g., 0.1–1 M NaOH (pH 13–14) [37], sometimes also with the addition of NaCl. Little focus has been spent on the adsorbent regeneration, with only a few studies investigating mechanism and strategies [20,24], even less analyzing in depth the desorption mechanism with HAIX [37]. No clear explanation has been provided on the role and desorption mechanism of NaOH and NaCl during the regeneration procedure. Some authors claimed that a mixture of NaOH and NaCl is needed to regenerate the AIX sites and the NPs, respectively [8,13]; others that NaCl is needed to remove the organics [7] and to replace the OH^- in the AIX sites with Cl^- [7,38]; others that NaOH alone would suffice [9,39]. Kumar et al, 2018 [20], pointed out that HAIX regeneration may affect the NPs speciation, and decreasing adsorption performances already after few regeneration cycles. It is crucial for the economics of the process to better understand regeneration and its effect on the adsorbent, to be able to design a strategy to minimize use of chemicals, obtain a purer recovered phosphate stream and having a long-lasting adsorbent. This work aims at better understanding the phosphate desorption process and interaction between the NaOH and both the NPs and the AIX backbone.

Finally, doping iron oxide could help improving the performances and stability of HAIX. Doping is a technique popular in the semiconductor and catalysis fields [40–44], which consists in adding one or more impurities (via inclusion or substitution) into the structure of a material. This allows to manipulate the material properties, like conductivity, magnetic properties, surface properties, and so on [45–50]. Two recent studies from our group on goethite (a highly stable iron oxide) NPs doping showed Zn-doped goethite to be promising for P recovery [51,52], improving the surface properties (e.g., point of zero charge) and adsorption capacity of goethite. However, these NP's have never been tested in an AIX resin.

In this study, two different syntheses procedures for HAIX have been compared, and a successful impregnation of Zn-doped iron oxide was achieved. Mössbauer spectroscopy was employed to obtain a finer and more accurate characterization of the NPs Fe phases in HAIX. The synthesized HAIX were tested and compared to a commercial HAIX and a commercial AIX, both in synthetic P solution and P-spiked wastewater, for three adsorption–desorption cycles. These experiments aim to: 1) investigate the feasibility of applying Zn-doped goethite NPs in the form of HAIX; 2) improve the understanding of the roles of the AIX backbone and of the NPs during adsorption, and how the different conditions can affect result interpretations; 3) investigate the regeneration procedure and phosphate desorption mechanism; 4) improve the information on the nature and fate of the iron oxide NPs in HAIX, by means of Mössbauer spectroscopy.

Table 1
Characteristics of the wastewater collected from the WWTP in Leeuwarden.

Parameters	Values
Temperature (during adsorption)	25 °C
pH	7.4–7.6
Conductivity	1.2 ± 0.2 mS cm^{-1}
Phosphorus (P)	0.100 ± 0.01 mg/L
Calcium (Ca)	60 ± 1 mg/L
Magnesium (Mg)	20.0 ± 0.2 mg/L
Sulphur (S)	9.2 ± 0.2 mg/L
Nitrate (NO_3^-)	2.3 ± 0.1 mg/L
TOC	12 ± 1 mg/L
TIC	73 ± 1 mg/L
Silicon (Si)	12.0 ± 0.1 mg/L
Zinc (Zn)	0.072 ± 0.007 mg/L
Iron (Fe)	0.064 ± 0.008 mg/L

2. Materials and methods

2.1. Chemicals

Iron sulphate ($Fe(SO_4)\cdot 6H_2O$) and 3-(N-morpholino)-propane sulfonic acid (MOPS) were purchased from Sigma-Aldrich (The Netherlands). Potassium dihydrogen phosphate (KH_2PO_4), potassium permanganate ($KMnO_4$), sodium chloride (NaCl), sodium hydroxide (NaOH), hydrochloric acid (HCl) and nitric acid (HNO_3) were purchased from VWR (The Netherlands). Iron chloride ($FeCl_3\cdot 6H_2O$) and zinc chloride ($ZnCl_2\cdot H_2O$) were purchased from Alfa Aesar (Germany).

2.2. Adsorbents

2.2.1. Commercial adsorbents

The anion exchange resin A500Plus (A500+) was obtained by Purolite GmbH (Germany), and it often constitutes the backbone of HAIX adsorbents [7–9,13,26,28,53]. The commercial HAIX adsorbent selected as a reference, LayneRT^{TM} (Layne) [7–9,13,25,28] of Layne Christensen Co (United States), was obtained via Aquacare ('s-Hertogenbosch, The Netherlands). Table S1 shows the main characteristics of these commercial adsorbents.

2.2.2. Synthesized adsorbents

The synthesis procedure consisted of impregnating pure and doped iron hydroxide nanoparticles in the A500+ resin following two different procedures.

The first procedure was adapted from the patent of SenGupta et al., 2007 [53], which is the basis of HAIX used for As removal from drinking water [262]. In short, about 15 g of A500+ was weighed and thoroughly washed in Deionized Water (DW), and a 2 L solution of 500 mg/L $KMnO_4$ concentration and a 0.5 L CO_2-free solution 5 %w/v $FeSO_4$ were prepared. The resins were first immersed in the $KMnO_4$ solution and let to shake for 30 min, then removed and thoroughly washed in DW. The $KMnO_4$ impregnated resins (now of a violet color) were then immersed in the $FeSO_4$ solution and let to shake for 4 h. The resins (now of a dark brown color) were then separated from the solution and thoroughly washed in DW. The whole procedure was performed for a total of 3 impregnation cycles, to increase the Fe loading. The so-synthesized adsorbent is referred to as R_{Mn}[Fe]. An attempt to embed 5 %at. Zn/(Zn + Fe) doped iron hydroxide NPs via this procedure was performed without success, hence no follow-up experiments were performed with this type of adsorbent.

The second synthesis procedure was adapted from Kociołek-Balawejder et al., 2017 [53]. In short, about 10 g of A500+ was weighed and thoroughly washed in DW. The resins were then immersed for 24 h in 100 mL of 0.5 M $FeCl_3$ in 5 M HCl solution. Then, the resins were filtered out via Büchner filtration and immersed in 50 mL of 1 M NaCl in 1 M NaOH solution for 24 h to promote the iron hydroxide precipitation within the resin. The resins (now of a brownish color) were separated and thoroughly washed in DW. The so-synthesized adsorbent is referred to as R_{HCl}[Fe]. Similarly, this procedure allowed for Zn-doped iron hydroxide precipitation within the resin, by adding $ZnCl_2$ to the $FeCl_3$ solution, in this case to obtain a doping percentage of 5 %at. Zn/(Fe +

Zn). This sample is referred to as R_{HCl}[Fe+Zn].

2.2.3. Adsorbent characterization

The elemental composition of all HAIX was investigated with two methods. Firstly, via HNO_3 (69 %) microwave digestion (MWD) with a Milestone Ethos Easy digester with a SK-15 High-Pressure rotor, followed by elemental analysis with a Perkin Elmer Optima 5300 DV Inductively Coupled Plasma Optical Emission Spectroscopy (ICP). Secondly, with a JEOL JSM-6480 LV Scanning Electron Microscope (SEM) equipped with an Oxford Instruments x-act SDD Energy Dispersive X-ray (EDX) spectrometer. Samples were coated with <10 nm of gold to make them conductive. The SEM images were analyzed with the JEOL SEM Control User Interface software and while the EDX data were processed with the Oxford Instruments Aztec software.

The Fe speciation in all HAIX was investigated using Mössbauer spectroscopy (MS). Transmission ^{57}Fe MS spectra were measured at 300 K (room temperature), 120 K (set-up thermalization with liquid nitrogen) and 4.2 K (liquid helium). The lower temperatures are needed as they promote the Zeeman splitting of Mössbauer spectral lines, allowing for better identification of (super)paramagnetic phases [34]. The MS spectra were collected with conventional constant acceleration or sinusoidal velocity spectrometers using a ^{57}Co (Rh) source. The MS spectra, calibrated to α-Fe, were analyzed with MossWinn 4.0 software [54], to retrieve the different relevant parameters (explained in section S2).

2.3. P solutions

The adsorption experiments consist of adsorption kinetics experiments and adsorption–desorption experiments. For both types of experiments, all adsorbents (A500+, Layne, R_{Mn}[Fe], R_{HCl}[Fe] and R_{HCl}[Fe+Zn]) were tested at an adsorbent concentration of 2 g/L in two water scenarios: in P synthetic solution and in P-spiked wastewater (ww).

First, a 500 mg/LP stock solution was prepared by dissolving KH_2PO_4 in Demineralized Water (DW), adjusting the pH to around 7 using NaOH/HCl. For the experiments in synthetic solution, a proper dilution was performed adding 20 mM MOPS as a pH buffer, adjusting the pH with NaOH/HCl to 7.2, within the pH range 6–8 of interest for surface waters and wastewater treatment plant (WWTP) effluents. For the experiment with P-spiked ww, the wastewater was collected from the sewage effluent of the WWTP in Leeuwarden, and Table 2 reports its main characteristics (composition expressed as total concentrations). The wastewater was filtered via Büchner filtration and spiked by slowly adding a proper aliquot of the P stock solution while stirring. The wastewater pH after P-spiking remained between 7.4 and 7.6, and it was measured after adsorption, with final pH values between 8.00 and 8.5.

The solutions for the adsorption tests were analyzed before and after adsorption with the ICP for the elemental composition, a Metrohm Compact IC Flex 930 ion Chromatograph (IC) for the ionic composition (in both cases, IC and ICP samples were filtered with a 0.45 μm hydrophilic filter) and a Shimadzu TOC-L CPH (CHECK) to assess the total organic carbon (TOC), total inorganic carbon (TIC) and hence the total carbon (TC) content. All data were then analyzed using Microsoft Excel.

2.3.1. Adsorption kinetics

The adsorption kinetics experiments were performed in batch mode, with both water scenarios (synthetic water and wastewater) for two main reasons. Firstly, to assess the time required for the adsorbent to reach equilibrium, to design the adsorption–desorption experiments. Secondly, to monitor over time the different adsorbent behavior in the two different scenarios. For both scenarios, the initial P concentration was of 25 mg/L, which is rather high, but it was chosen to allow for relatively frequent sampling with small volumes of solution, to minimize perturbations to the system. The experiments were performed in duplicates plus blank (or control), and water samples were collected after 15, 30 min, 1, 2, 4, 22, 24, 28, 48, 52, 71 h, 1, 2, 3, 4 weeks and the P content analyzed with ICP. The amount of P adsorbed per mass of adsorbent was calculated via:

$$q_i(t_i) = \frac{c_0(t_0) - c_i(t_i)}{m} V \quad (1)$$

where q_i [mg g^{-1}] is the adsorbent loading at the time t_i, c_0 [mg/L] is the initial P concentration, c_i [mg/L] is the P concentration at time t_i, m [g] is the adsorbent mass and V [L] is the solution volume. For each q_i, the change in volumes due to sampling were taken into account.

The results were analyzed with two models, the Pseudo-First Order (PFO) [55,56] and Pseudo-Second Order (PSO) [57] kinetics, to investigate the behavior of the different adsorbent and to estimate the equilibration time, t_{eq}, and t_{95}, at which 95 % of equilibrium is reached.

The PFO kinetic model, based on the assumption that the adsorption limiting factor is the concentration of the adsorbate, usually describes better physisorption. The PSO kinetic model, based on the assumption that the adsorption mechanism limiting factor is the adsorbent capacity, usually describes better chemisorption (in which a chemical bond forms between the adsorbent and the adsorbate). The two models are respectively described by the equations:

$$q(t) = q_{eq}(1 - e^{-k_1 t}) \quad (2)$$

$$q(t) = \frac{k_2 q_{eq}^2 t}{1 + k_2 q_{eq} t} \quad (3)$$

where t [h] is the time, $q(t)$ [mg g^{-1}] is the adsorbent loading at time t, k_1 [g mg^{-1} min^{-1}] is the kinetic rate constant of the PFO kinetic model, k_2 [g mg^{-1} min^{-1}] is the kinetic rate constant of the PSO kinetic model, and q_{eq} [mg g^{-1}] is the adsorbent loading at equilibrium. The fittings were performed using the Microsoft Excel Solver add-in, and the goodness of the fit assessed both evaluating the Root Mean Squared Percentage Error (RMSPE).

2.4. Adsorption-desorption tests

The adsorption–desorption experiments were performed for 3 cycles in batch mode (triplicates plus blank) with both water scenarios, at an initial P concentration of 5 mg/L.

The equilibration time was 5 days and the amount of P adsorbed was estimated after each cycle using equation (1) and plotted in histograms. After adsorption, the solution was removed, the adsorbent washed with

Table 2
Adsorption kinetics fitting results.

Sample	PFO			PSO			t_{95} [h] *(based on PFO)*
	k_1 [g mg^{-1} min^{-1}]	q_1 [mg g^{-1}]	RMSPE	k_2 [g mg^{-1} min^{-1}]	q_2 [mg g^{-1}]	RMSPE	
A500+	0.005	8.8	0.112	0.0005	9.3	0.158	11
Layne	0.010	4.1	0.116	0.003	4.2	0.123	5
R_{Mn}[Fe]	0.005	5.1	0.106	0.001	5.4	0.143	10
R_{HCl}[Fe]	0.004	9.5	0.126	0.0004	10.1	0.159	12
R_{HCl}[Fe+Zn]	0.004	9.8	0.165	0.0003	10.5	0.190	14

DW (3 × 50 mL, shaken for couple of minutes), and exposed for one day to a 0.01 M NaOH solution (pH 12), which was reused over the 3 cycles. The low pH, compared to the higher pH 13–14 usually employed [7,9,37,53], was chosen to enhance any difference in the desorption behavior (and to promote faster saturation). After desorption, the NaOH solution was analyzed and the adsorbents were washed with DW several times (3 × 50 mL, shaken for couple of minutes each time), until the DW pH dropped to around 7, to then start a new adsorption cycle. Also, the concentration of P in the DW washings was measured.

After the last regeneration cycle, the adsorbent was regenerated with 1 M NaOH solution (pH 13.7) to fully regenerate the adsorbent and estimate the residual P adsorbed.

3. Results

3.1. Adsorbents characterization

The results of the ICP analysis of the MWD samples are shown in Table S2 and the Fe content is shown in Fig. 1. LayneRT and R_{Mn}[Fe] display similar Fe, Mn and S content. R_{HCl}[Fe] and R_{HCl}[Fe+Zn] adsorbents display similar Fe content, lower compared to Layne and R_{Mn}[Fe]. For R_{HCl}[Fe+Zn], the Zn content was the 5 %at. targeted.

SEM-EDX analysis (see section S4.) shows a significant and even Fe distribution for all HAIX, and forR_{HCl}[Fe+Zn], an even distribution of Zn, close to 5 %at. compared to the Fe. Samples A500+, R_{HCl}[Fe] and R_{HCl}[Fe+Zn] display a significant presence of homogeneously distributed Chlorine, while Layne and R_{Mn}[Fe] showed the same for Sulfur with only traces of Chlorine.

Mössbauer characterization results are reported in Figure S1 and Table S3 and show the Fe-based NPS in HAIX, mainly consisting of superparamagnetic goethite (Fe^{3+}). Mössbauer results also suggest that R_{HCl}[Fe+Zn] contains Zn-doped goethite (see section S5.2).

3.2. Adsorption kinetics

3.2.1. P synthetic solution

The long-term (4 weeks) adsorption kinetics graphs in P synthetic solution are showed in section S6, and the fitting results are reported in Table 2. Fig. 2 shows the kinetics results within the first 24 h (to show the reached plateau) and 10 h (to better zoom into the first adsorption timeframe and better compare the data agreement with the two kinetics models). The fitting was performed over the entire time range (4 weeks), providing more data points and higher confidence on the maximum loading at equilibrium. The PFO model showed slightly lower RMSPE than the PSO and was used to estimate t_{95}, as the PSO seemed to largely overestimate q_{eq} and t_{eq}. The faster sample to reach equilibrium was Layne, which reached 95 % of equilibrium within 5 h, followed by

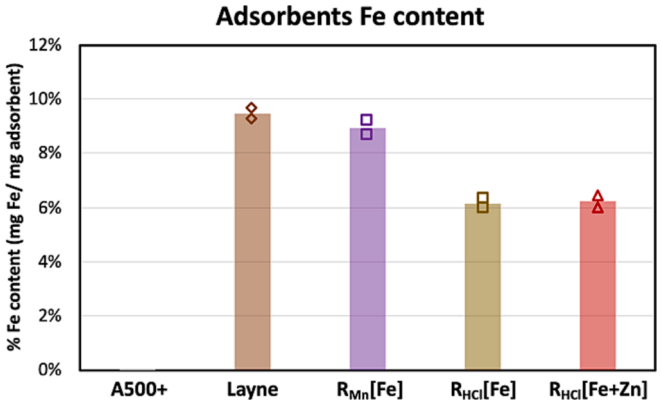

Fig. 1. Fe content of the different adsorbents, as determined by ICP analysis of the MWD samples.

R_{Mn}[Fe], A500+, R_{HCl}[Fe], between 10 and 11 h, and lastly R_{HCl}[Fe+Zn], around 14 h. Samples A500+, R_{HCl}[Fe] and R_{HCl}[Fe+Zn] show higher P capacities (8.3, 9.0 and 9.3 mg g^{-1}, respectively), about double that of Layne and R_{Mn}[Fe] (4.1 and 5.1 mg g^{-1}, respectively).

3.2.2. P-spiked wastewater solution

The long-term (4 weeks) adsorption kinetics graphs in P-spiked wastewater are shown in S6 and display a multistep trend. Fig. 3 shows the kinetics within the first 24 h, which is closer to the timescale of interest for application, also according to the kinetics results in P synthetic solution. Within 24 h, all the adsorption curves saturate around the same P loading range. The P loading follows the trend: R_{HCl}[Fe+Zn] > R_{HCl}[Fe] > R_{Mn}[Fe] > A500+, Layne.

Fig. 4 shows the comparison between the adsorption kinetics in P synthetic solution and in P-spiked wastewater.

3.3. Adsorption-desorption tests

3.3.1. P synthetic solution

The averaged results of the three adsorption–desorption cycles in P synthetic solution are shown in Fig. 5 for adsorption, and Fig. 6 for desorption. All samples showed similar P loadings in the first cycle, around 2 mg g^{-1}. The adsorbents behaved differently from the second cycle. A500+, R_{HCl}[Fe] and R_{HCl}[Fe+Zn] maintained almost the same adsorption performances throughout the three cycles (deviation within 6 %), while Layne and R_{Mn}[Fe] faced a decrease compared to the first cycle of about 50 % and 38 %, respectively, in the second cycle, and up to 61 % and 41 %, respectively, in the third cycle.

Fig. 6-right shows the pH values of the regeneration solution after each desorption cycle. The initial pH value was 11.9. All samples show similar pH drops in the first two desorption cycles of 0.2–0.5. In the third cycle, A500+, R_{HCl}[Fe] and R_{HCl}[Fe+Zn] showed a pH drop down to pH 9.0–9.7, while Layne and R_{Mn}[Fe] reached pH 11.2–11.4.

Fig. 6-left shows the averaged percentages of desorbed P compared to the total P loading after each adsorption cycle. The desorbed P takes into account the P detected in the regeneration solution and in the DW washings, and is cumulative, as the regeneration solution was reused. No desorbed P was detected for A500+, R_{HCl}[Fe] and R_{HCl}[Fe+Zn] until the third desorption cycle, which accounted for<4 % of the total P adsorbed. Layne also did not show any desorbed P after the first cycle, while in the second and third desorption cycles, P was detected up to 12 % and 20 %, respectively. Conversely, R_{Mn}[Fe] desorbed P in all cycles, from 10 % to 34 %.

Regeneration at pH 14 returned all the P retained during the regenerations at pH 12 for all samples.

3.3.2. P-spiked wastewater

The averaged results of the three adsorption–desorption cycles in P-spiked ww are shown in Fig. 7 for the adsorption, and Fig. 8 for the desorption. In the first adsorption cycle, all HAIX showed similar P adsorption performances, with P loading between 1.5 and 2.1 mg g^{-1}, which is about double the P loading of A500+ of 0.8 mg g^{-1}. The second cycle showed a drop in P loading for all samples: 40 % for A500+; around 70 % for Layne and R_{Mn}[Fe]; around 50 % for R_{HCl}[Fe] and R_{HCl}[Fe+Zn]. Finally, in the third cycle, a further reduction in P loadings compared to the first cycle was observed: 65 % for A500+; about 80 % for Layne and R_{Mn}[Fe]; about 70 % for R_{HCl}[Fe] and R_{HCl}[Fe+Zn]. Note that the Zn-doped HAIX managed to adsorb on average more P than Layne and R_{Mn}[Fe], despite these having higher Fe content.

The results on competitive ions, TOC and inorganic carbon removal are reported in section S7.

Fig. 8-left shows the averaged percentages of desorbed P compared to the total P loading after each adsorption cycle. The amount of desorbed P is calculated as in section 3.3.1. Also in this case, no desorbed P was detected in the first cycle for all samples except for R_{Mn}[Fe] (around 8 %). However, this time all samples desorbed between 16 and 20 % of

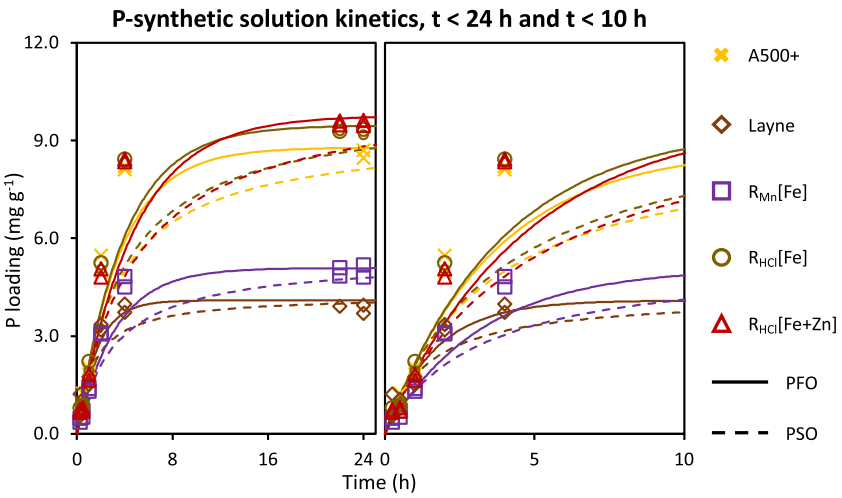

Fig. 2. Adsorption kinetics of all samples in P synthetic solution, within 24 h and 10 h. The solid and the dashed lines represent the PFO and the PSO fitting curves, respectively.

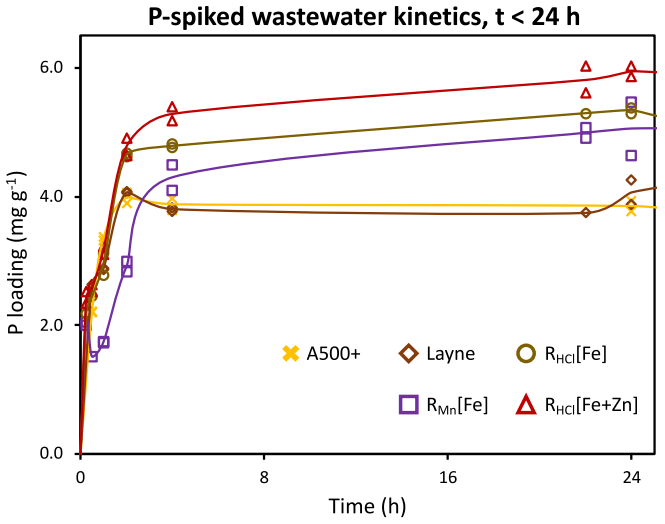

Fig. 3. Adsorption kinetics of all samples in P-spiked wastewater, within 24 h. The duplicate data are superimposed to the solid line representing the average trend.

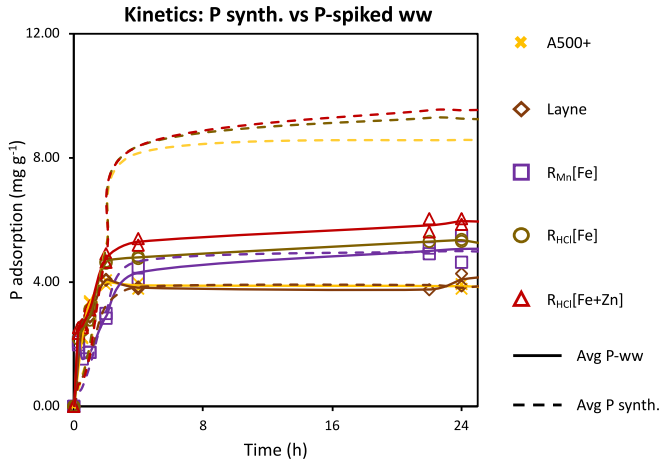

Fig. 4. Comparison between the kinetics in P synthetic solution and P-spiked wastewater, within the first 24 h. The markers and solid lines represent the duplicate data and average trend in P-spiked wastewater, respectively. The dashed lines represent the average trend in P synthetic solution.

the adsorbed P after the second regeneration cycle, and up to 26–38 % after the third regeneration cycle.

Fig. 8-right shows the pH values of the regeneration solution after each desorption cycle. Also in this case, the initial pH was 11.9, and showed minor decreases for all samples after the first two desorption cycles, 11.7–11.8 after the first and 11.2–11.7 after the second. However, after the third cycle, the desorption solution reached pH values between 10.0 and 10.4 for all samples, except Layne, which displayed a value of 11.2.

Regeneration at pH 14 returned all the P retained during the regenerations at pH 12 for all samples.

3.3.3. *Mössbauer analysis of regenerated samples*

Table S4 reports the fitting parameters of the MS spectra showed in Figure S8 of the fully regenerated (pH 14) HAIX after the three adsorption–desorption cycles in synthetic P solution. The Fe speciation results are in agreement with the goethite phase for all HAIX.

Table S5 reports the fitting parameters of the MS spectra showed in Figure S9 of the fully regenerated (pH 14) HAIX after the three adsorption–desorption cycles in P-spiked wastewater. The Fe speciation results are in agreement with the goethite phase for all HAIX.

4. Discussion

4.1. *Samples characterization*

The results from MWD + ICP and SEM-EDX reported in section 3.1 show that the two synthesis procedures were both successful, and that it was also possible to obtain HAIX with Zn-doped iron oxide NPs (interestingly, only with the second procedure), with the targeted 5 %at. doping. R_{Mn}[Fe] and Layne achieved similar loadings, higher than R_{HCl}[Fe] and R_{HCl}[Fe+Zn]. This is most likely due to the fact that the first synthesis allows for three consecutive impregnation cycles, while the second allows only for a single impregnation cycle. Nevertheless, the second synthesis could be tuned to obtain Fe loadings similar to the first one (out from the scopes of this research). It is important to note that the Fe content does not provide a direct indication on the adsorption performances, as was observed by Zhang et al., 2008 [58]. Moreover, the fact that Layne and R_{Mn}[Fe], other than having similar Fe loadings, display also Mn and S content, suggests that both HAIX are synthesized with the same (or similar) synthesis procedure. SEM-EDX results show that the resin adsorption sites of Layne and R_{Mn}[Fe] are in sulfate form

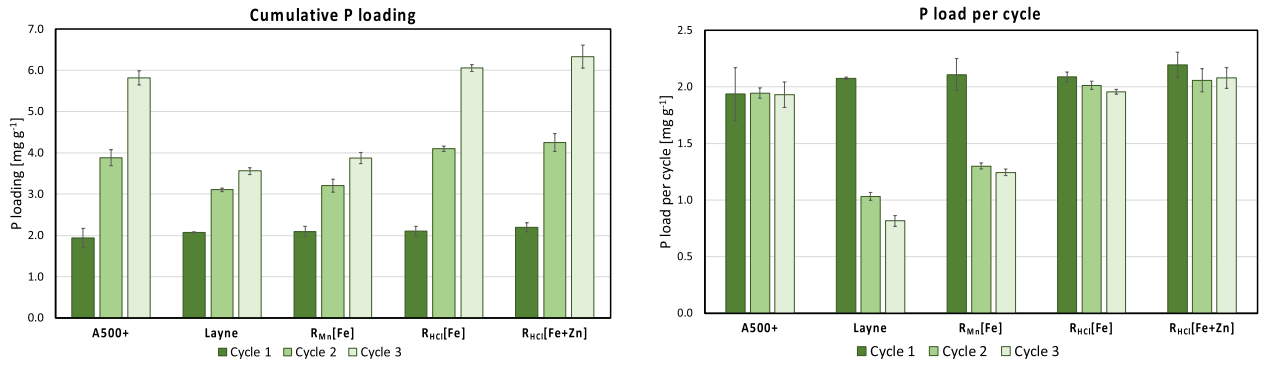

Fig. 5. Adsorption results in P synthetic solution for all adsorbents. Results are shown in terms of cumulative P loading cycle after cycle (left) and P loading per cycle (right).

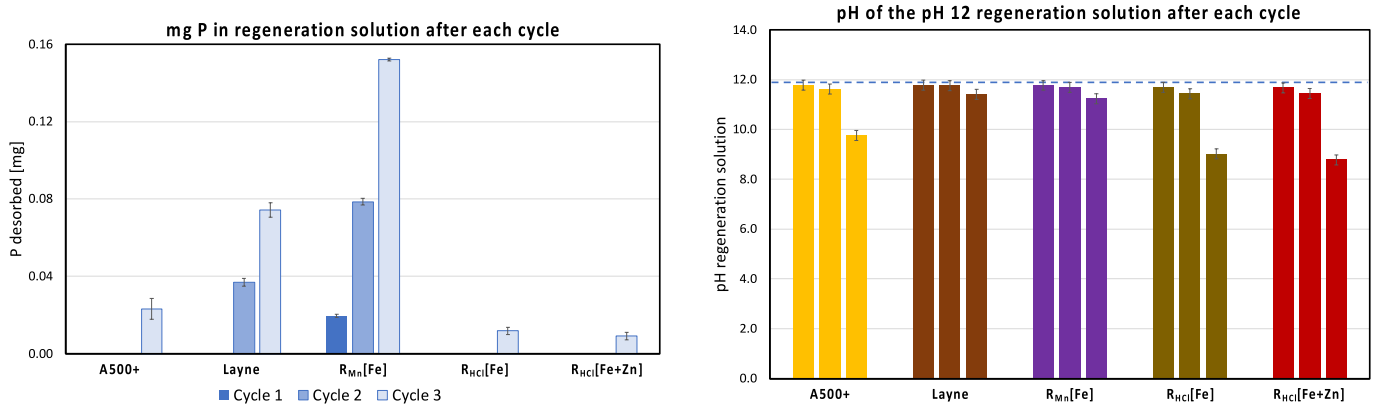

Fig. 6. P desorbed after each adsorption cycle in P synthetic solution, with respect to the total cumulative P loading (left); and pH value of the regeneration solution after each desorption cycle (right), with the dashed line representing the initial pH.

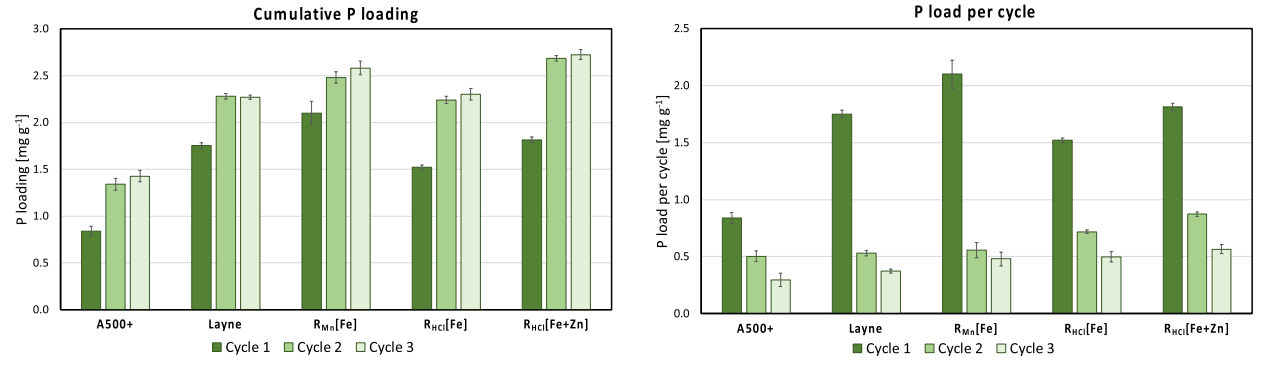

Fig. 7. Adsorption results in P-spiked wastewater for all adsorbents. Results are shown in terms of cumulative P loading cycle after cycle (left) and P loading per cycle (right).

([13]). Conversely, the adsorption sites of A500+, R_{HCl}[Fe] and R_{HCl}[Fe+Zn] are in chloride form. Hence, the adsorbents can be divided in two groups: S-based adsorbents and Cl-based adsorbents.

MS results, shown in section 3.1, show that all samples contained goethite NPs, with Layne and R_{Mn}[Fe] having NPs of smaller size compared to R_{HCl}[Fe] and R_{HCl}[Fe+Zn], and with the latter HAIXs containing other superparamagnetic iron oxide phases.

Layne shows the highest dispersion of "ultrafine" NPs of goethite (see section S5 for further details). This is in contrast to literature, where HAIX like Layne are claimed to consist of "non-crystalline iron oxides", "amorphous iron hydroxide", "hydrous ferric oxide" (or HFO) [3,4,6–9,11,26,29–33,35,36], or other similar inaccurate and generic terms [34], most likely referring to ferrihydrite. These interpretations arose from X-ray diffraction (XRD) measurements, which face limitations when dealing with ultrafine (<10–15 nm) and/or amorphous NPs. Only Sylvester et al., 2007 [33], hypothesized the possibility of the presence of the goethite phase in such adsorbents.

Similarly, R_{Mn}[Fe] also consists of fine goethite NPs of slightly bigger size compared to those of Layne.

Differently, R_{HCl}[Fe] and R_{HCl}[Fe+Zn] seem to consist of a mixture of goethite phases and/or ferrihydrite or other superparamagnetic phases. Results also suggest the NPs in R_{HCl}[Fe+Zn] consist in fact of a Zn-doped goethite phase..

The NPs size dispersion follows the order R_{Mn}[Fe] < R_{HCl}[Fe] < R_{HCl}[Fe+Zn], with the latter seemingly containing goethite NPs on average bigger than Layne and R_{Mn}[Fe].

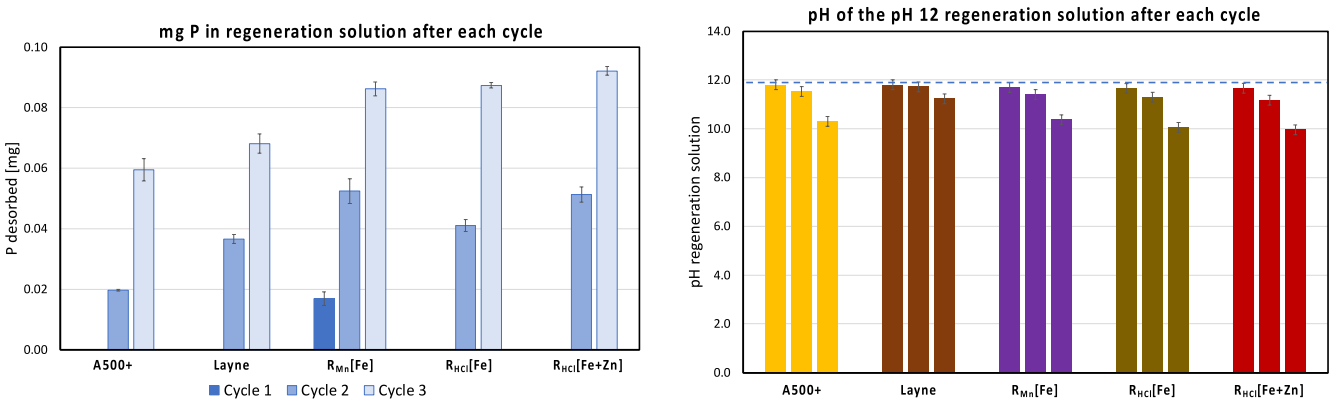

Fig. 8. P desorbed after each adsorption cycle in P-spiked wastewater, with respect to the total cumulative P loading (left); and pH value of the regeneration solution after each desorption (right), with the dashed line representing the initial pH.

These results suggest that both syntheses are successful to embed iron oxide NPs in AIX, although displaying different capabilities, from Fe loading, NPs sizes and size dispersion, possibility of doping. Further research to tune the outcome two syntheses is recommended to achieve higher control on the final product. Also, these observations suggest that a different strategy should be followed to successfully embed specific iron oxide NPs, e.g., Zn-doped goethite NPs, onto a support, in a controlled way. Such strategy should consist of a first NPs synthesis step, which would provide more control on the iron oxide NPs phase and properties, and a second step in which either these NPs are blocked on a support, or the support is "built around" such NPs.

4.2. Adsorption kinetics

The fit results from the adsorption kinetics in P-synthetic solution, reported in section 3.2.1, show for all samples a (slightly) better agreement with the PFO kinetic model compared to the PSO kinetic model, both in terms of RMSPE and agreement between the curve and the data trend. This is most likely due to the relatively high initial P concentration [59,60]. The (slight) better agreement with the PFO model does not necessarily mean that physisorption is the only adsorption mechanism taking place for all samples, but rather that the limiting factor during adsorption was the P concentration. Surely, physisorption takes place, due to the AIX backbone. The extent of NPs chemisorption contribution needs to be determined. Hence, it is important to remind that the kinetic model fitting does not tell anything on the adsorption pathway or mechanism, which can only be determined with direct measurements [61].

Despite the similarities in removal behavior, there is a significant difference in the P adsorption performances. According to the results in section 3.2.1, t_{95} for the different adsorbents followed the trend Layne < R_{Mn}[Fe], A500+, R_{HCl}[Fe] < R_{HCl}[Fe+Zn]. A500+, R_{HCl}[Fe] and R_{HCl}[Fe+Zn] show higher P adsorption capacities about double those of Layne and R_{Mn}[Fe]. On the one hand, it looks striking that A500+ performed similarly to or even better than the other HAIX, despite the absence of iron hydroxide NPs. On the other hand, the role of iron hydroxide NPs is to improve adsorption selectivity, not the capacity. Hence A500+, being an AIX, is expected to physisorb anions, as is phosphate, and to perform well especially when phosphate is the only anion in solution.

The difference in adsorption capacities between the S-based and the Cl-based adsorbents is related to the counterion form in the resin (or at least, in P loading during the first adsorption run, being adsorption kinetics a single-run experiment, since in the long run, after multiple adsorption–desorption cycles, the effect of the counterion on the resin backbone will become less relevant). Before diving into this discussion point, a premise on AIX first, and pH conditions next, are necessary. First, AIX with type I quaternary ammonium sites are known to have a higher selectivity for (more hydrophilic) divalent anions over monovalent anions, if there are closely spaced anion-exchange sites [17,18,62,63]. It was shown that that these AIX have higher selectivity for SO_4^{2-} over Cl^- [17,18,64]. Concerning NO_3^-, the selectivity depends on the hydrophobicity of the resin (mainly determined by the length of the quaternary ammonium radicals). In this case, type I (trimethyl) is the shortest, making the resin less hydrophobic, hence more selective for SO_4^{2-} than for NO_3^-, according to [13,17,18,62], and opposed to [9]. Second, adsorption is performed at pH 7.2, coinciding with the second pK_a of phosphate [65], meaning that its speciation is dynamically evenly distributed as the monovalent and divalent phosphate, $H_2PO_4^-$ and HPO_4^{2-}, respectively.

These considerations help understanding the differences in adsorption mechanism between the S-based and the Cl-based adsorbents (as previously said, at least for the first adsorption run)). In the case of the Cl-based ones, phosphate may on average adsorb both in the monovalent and divalent state, either via physisorption by the resin, exchanging with Cl^-, or via chemisorption by the NPs. Possibly, only the divalent phosphate is adsorbed on the backbone, with MOPS restoring the speciation in solution. In the case of the S-based adsorbents, both forms can chemisorb onto the NPs, while only the divalent phosphate is likely to exchange for SO_4^{2-}, depending on its concentration. For the S-based resins, Martin et al, 2018 [13], suggested that P adsorption in Layne is due 90 % to the NPs and 10 % to the resin backbone. Thus, Layne and R_{Mn}[Fe] get quickly saturated (as supported by the t_{95} values), explaining 50 % difference in loading compared to the Cl-based adsorbents. It could be concluded that for the Cl-based adsorbents physisorption is the dominant process, while for the S-based adsorbents, either chemisorption is the dominant process.

This is further corroborated by the results obtained in P-spiked wastewater in section3.2.2,

as all the adsorption curves converged around the same range of values. This is due to the higher competition (e.g., nitrates, sulphate, silicates, carbonates, chloride, organics) taking place in the more complex water matrix. R_{HCl}[Fe+Zn] still shows the highest P adsorption capacity, followed by R_{HCl}[Fe] and R_{Mn}[Fe], while A500+ and Layne showed the lowest loadings. Nevertheless, R_{Mn}[Fe] and Layne kept a similar loading as observed in synthetic solution. As the selectivity for P is determined by the presence of the NPs, this further supports the hypothesis that chemisorption (adsorption onto NPs) was the dominant adsorption mechanism in the P-synthetic solution for these samples, in agreement with [13]. Conversely, the performance drop observed for the Cl-based adsorbents further support the idea that physisorption was the dominant adsorption mechanism in P-synthetic solution for these samples. Moreover, the higher performances of R_{HCl}[Fe+Zn] and R_{HCl}[Fe] compared to A500+ can be ascribed to the NPs, which

provided higher selectivity for P.

4.3. Adsorption-Desorption results

The results from the adsorption–desorption experiments in section 3.3 show different adsorption behaviors. The results in P-synthetic solution (section 3.3.1) display similar performances for all adsorbents, with P loadings around 2 mg g^{-1} (C_{eq} 1 mg g^{-1}), with the HAIX generally performing better than A500+. This behavior goes against what was observed in the kinetic experiments. This is due to the lower P starting concentration, and this further highlights the importance of the choice of the initial conditions when performing adsorption experiments. Looking at the P loading per cycle (Fig. 5-right) and comparing this with the desorption results (Fig. 6), one notices an unexpected behavior of the Cl-based adsorbents. Firstly, no P desorption was obtained between each adsorption cycle (only < 4 % total P was desorbed after the third adsorption cycle). Previous studies with iron oxide NPs [52,66] showed that already at pH 12.6, desorption reached values above 65 %, up to 80, suggesting that this might be due to the resin backbone, perhaps able to accommodate more phosphate. Second, despite no P desorption was observed in-between the three adsorption cycles, the adsorbent managed to maintain the same P loading at each cycle. The regeneration at pH 14 returned all the (accumulated) adsorbed P, proving indeed that these adsorbents kept performing as shown in Fig. 5. This behavior goes against what usually is observed in adsorption experiments. Hence, something is happening when exposing the adsorbents to the regeneration solution. The detailed reasoning is provided for the A500+ case in section S9), and extended to the HAIX afterwards.

In short, what is happening is that passing from pH 7.2 to 12, the phosphate speciation changes, increasing in valency, hence favoring P re-adsorption (or stronger adsorption) onto the resin backbone, releasing further Cl^- and preventing P desorption. When going back to pH 7.2 for the successive adsorption cycle, the phosphate speciation goes back to a lower valency. This frees some adsorption sites, which eventually get compensated with OH^- from water molecules, becoming more accessible to the new incoming P. This causes a lower buildup of Cl^- molecules in water, while the MOPS compensates for the OH^-. Once saturation is almost reached (in this case, after the third adsorption cycle), during regeneration, there are less available sites to re-adsorb P at pH 12, and hence a small P desorption is observed.

A similar phenomenon might have happened for R_{HCl}[Fe] and R_{HCl}[Fe+Zn], with the difference that some phosphate might have desorbed from the NPs, getting then physisorbed by the resin (and perhaps adsorbed back onto the NPs).

In the case of Layne and R_{Mn}[Fe], a similar reasoning can be applied, with the differences related to the fact that they have an S-based AIX. In fact, their backbone should physisorb P in a limited manner [13], due to the higher affinity for sulfate than for mono- and divalent phosphate [19]. In the first regeneration cycle, only the chemisorbed P onto the NPs might have desorbed, only partially re-adsorbing onto the resin. Hence, saturation is rapidly reached, hence promoting effective P desorption already after the second (or even first) cycle.

Surely, these results highlight that there was a flaw in the experimental design, as the pH 12 regeneration did not manage to (efficiently) desorb P. Nevertheless, it provided insights for a better understanding of the interaction between an alkaline regeneration solution and a P-loaded AIX-based adsorbent. First, it is important to consider that not fully saturated adsorbents can still show high or even constant adsorption performances, irrespective of a successful regeneration. Second, while lower pH values during regeneration can still lead to P desorption for iron hydroxide NPs [52,66], this does not apply to HAIX adsorbents. Third, even though OH^- has a low affinity for the resin adsorption sites, it is not true that a highly concentrated alkaline solution cannot be used to regenerate HAIX adsorbents, as previously suggested [13]. In fact, in our case, the regeneration at pH 14 managed to fully desorb all the P accumulated from all adsorbents, A500+ included, in agreement with what reported by others [7–9,20]. Although challenging, tuning the regeneration procedure to only desorb the chemisorbed P would lead to a purer recovered P-based product.

Fig. 9, shows a simplified representations and version of the proposed reaction schemes for the different adsorbents, for the experiments in synthetic solution (i.e., with low quantities of competing ions).

In a complex media (e.g., wastewater, surface waters), similar adsorbent behavior and adsorption mechanisms may be expected, but taking into account the different affinities of the resin backbone and nanoparticles for the different ion species (and their concentrations) [19]. In this case, the level of complexity is too large to propose a similar simplified model, and further research is hence recommended for developing such a model.

Moving to the results in P-spiked ww, in section 3.3.2, the fundamental role of the NPs for P selectivity becomes more evident. In fact, in the first cycle, all HAIX maintained adsorption performances close to those observed with synthetic solution. The average decrease in P adsorption for Layne and R_{Mn}[Fe] were 15 % and 0 %, respectively, while for R_{HCl}[Fe] and R_{HCl}[Fe+Zn] were 27 % and 18 %, respectively. Conversely, A500+ faced an average decrease in P adsorption of 57 %. A comparison between the results in P synthetic solution and P-spiked wastewater are shown in Fig. 10. These results further prove that the iron oxide NPs provide higher selectivity.

Moreover, the results for Layne and R_{Mn}[Fe] support what was hypothesized in the kinetic study, that the dominant adsorption mechanism for them was chemisorption (or at least, inner-sphere complexation onto NPs). This is partially in agreement with what was observed for Layne by Martin et al., 2017 [13]. From the second cycle, all samples show a decrease in adsorption performances, caused by the combination of competitive compounds and inefficient P desorption. Interestingly, while in the first cycle no P desorption was observed (again with the exception of R_{Mn}[Fe]), 16–20 % of desorbed P was detected for all samples already from the second desorption cycle, up to 26–38 % in the third cycle. Two main reasons could explain this different behavior for the Cl-based adsorbents. First, the competitive ionic species are saturating the adsorption sites, not allowing the phosphate speciation shift and further exchange with Cl^- to the extent observed in the P synthetic solution experiment, causing P to get desorbed earlier. Second, TOC removal was observed (see Figure S7), most likely consisting of adsorption of humic substances, known to interact with IEX and iron (hydr)oxides, and to actively adsorb P [67–71]. Most likely, during regeneration, a fraction of this bound P might have desorbed from or together with the humics. It is also interesting to notice that after the third regeneration, the alkaline solution remained at pH > 10 for all samples, without any abrupt drop.

Unfortunately, no values for Cl^- or SO_4^{2-} are available for the synthetic solutions, preventing a complete mass balance to definitively prove the adsorption–desorption mechanism suggested above.

The results on competitive adsorption in wastewater are reported in section S7 and are briefly discussed here. Anions adsorption was in general greater for the adsorbent in chloride form, compared to that in sulfate form, and decreased throughout the three cycles, probably as a consequence of the unsuccessful desorption. Sulphate adsorption was observed in the Cl-based adsorbents, supporting the higher affinity of these resins for sulfate, compared to chloride. Sulphate desorption was observed for Layne and R_{Mn}[Fe], instead, probably coming from retained sulfate after the synthesis procedure, or exchange during P adsorption. Nitrates were removed by Cl-based adsorbents to a higher extent compared to the SO_4-form ones. Inorganic carbon, mostly carbonate, was also significantly removed by all samples. Silicates, which can cause surface precipitation on iron oxides, were removed only by the HAIX, not by the AIX, with R_{HCl}[Fe+Zn] displaying the highest Si removal.

Cations should be repelled by the adsorbents due to the Donnan exclusion effect. Nevertheless, cations retention or removal can happen due to the accumulation of negative charges, OH^- retention after

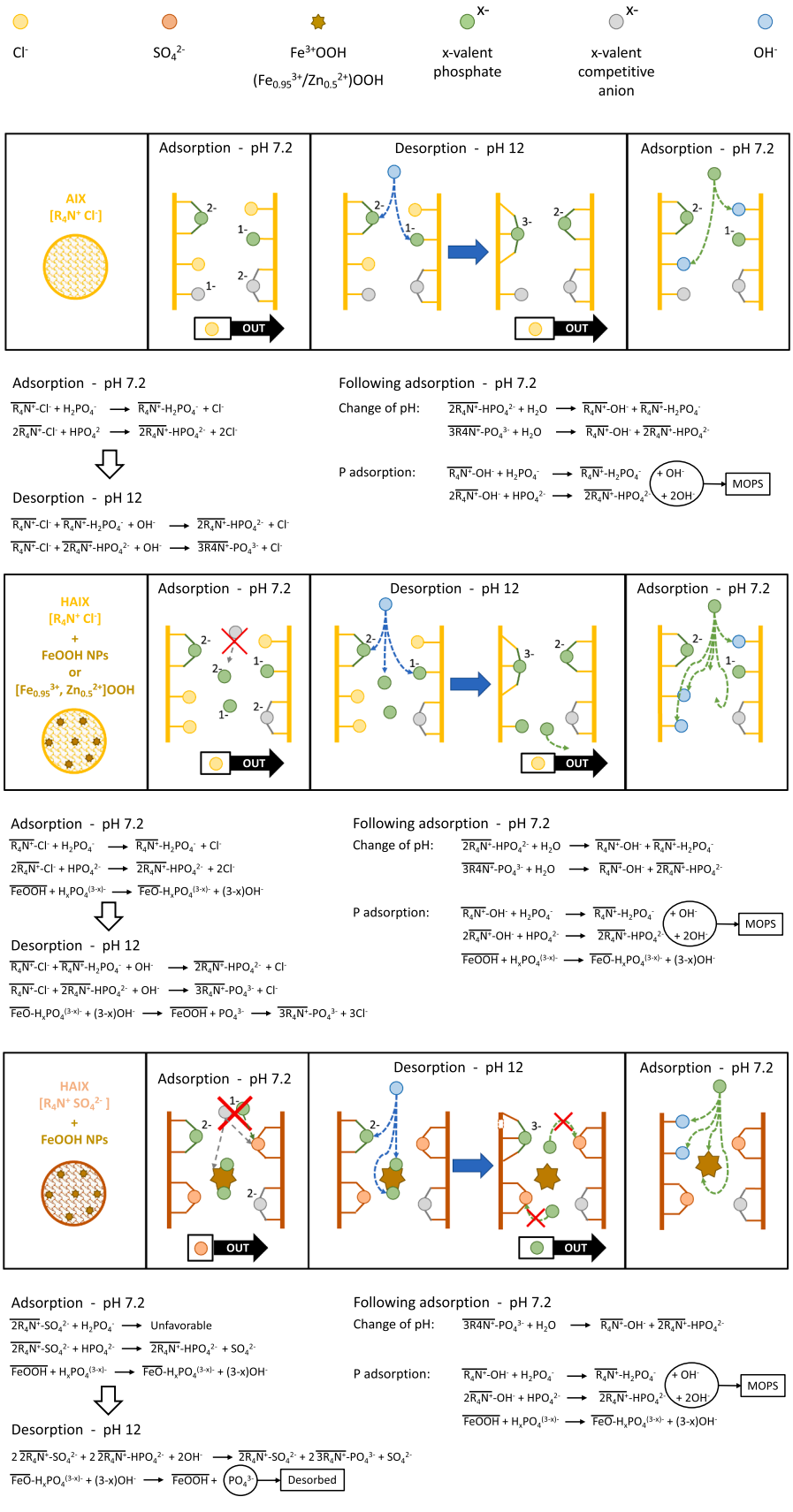

Fig. 9. Simplified representations and version of the proposed reaction schemes of the P adsorption–desorption-adsorption process in synthetic solution for the different adsorbents.

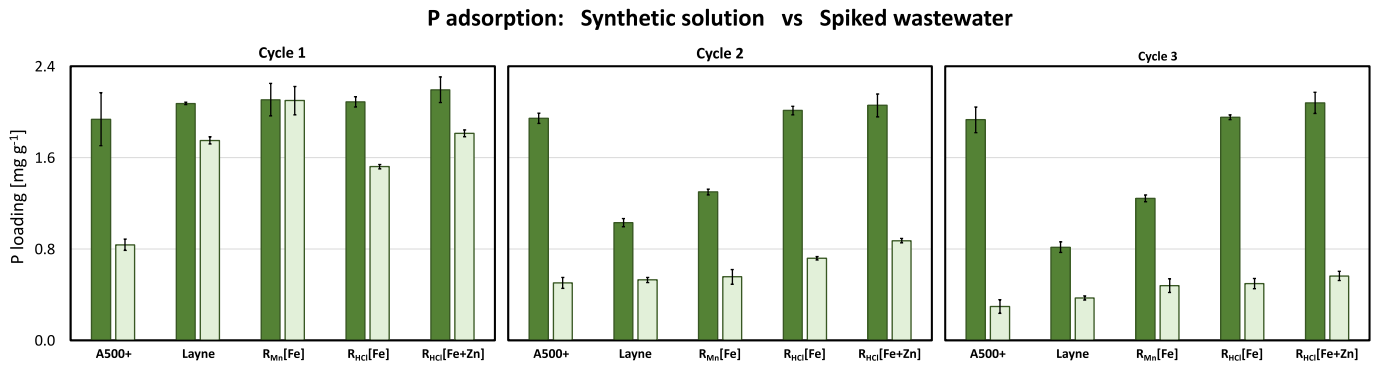

Fig. 10. Comparison between the P removal in P synthetic solution (full green) and P-spiked wastewater (shaded green), per cycle, for the different adsorbents.

desorption causing precipitation and presence of iron (hydr)oxides, which can remove anions as well as some divalent cations. First of all, Ca^{2+}, which can have both a favorable effect on adsorption, increasing the adsorbent positive surface charge and attracting more P [20,33], and a negative effect, causing carbonate and phosphate precipitation, obstructing pores and adsorption surface sites. It was observed to accumulate in the adsorbents, following the trend A500+ > Layne > R_{Mn}[Fe] > R_{HCl}[Fe] > R_{HCl}[Fe+Zn]. This suggests the occurrence of precipitation within the adsorbents, eventually requiring a further acid regeneration step [20,24]. Similar reasoning applies to magnesium, Mg^{2+}, although lower removal was observed. Iron, Fe^{3+}, and zinc, Zn^{2+}, were both removed, even though they were present in small concentrations, and zinc removal was lower for A500+ and R_{HCl}[Fe + Zn]. This suggests that zinc was mainly removed by the iron oxide NPs, as expected [72]. However, in the case of R_{HCl}[Fe+Zn], it needs to be investigated whether the Zn-doped NPs had lower affinity for Zn^{2+}, or whether the low uptakes comes from a balance between the Zn adsorbed by and that dissolved from the NPs.

Finally, for the organic carbon species, mainly consisting of humic substances, a considerable loading on the adsorbent was observed during the first cycle, which consistently reduced in the second and third cycles.

The MS analysis results of the regenerated HAIX showed in section S8 provide as main message that throughout the adsorption–desorption cycles, NPs crystal growth is taking place (e.g., increase in crystallite size, increase in NPs size, etc.). This could have happened either via dissolution and reprecipitation of NPs within the resin bead or via oriented attachment (or oriented agglomeration), which is a size-dependent mechanism [73–77], suggested to be promoted in water [75,78], even more at alkaline conditions [77] and by phosphate adsorption [76]. For R_{HCl}[Zn+Fe], it is unclear whether the Zn-doped goethite NPs are also dissolving, or transforming to other phases. Hence, further experiments are needed to verify the stability of such synthesized Zn-doped goethite nanoparticles in HAIX.

Samples R_{Mn}[Fe] used either in P synthetic solution or P-spiked wastewater, have also been analyzed with MS after the third regeneration at pH 12 (i.e., before the final pH 14 regeneration). They were selected as representative samples, since they showed the highest degree of NPs growth after pH 14 regeneration. The results (shown in section S10), compared to the MS results after pH 14 regeneration, supports that high alkaline conditions are the main driver for NPs growth (either via dissolution and reprecipitation within the resin bead, or mediated by oriented attachment).

Overall, the MS results highlight that NPs crystal growth is taking place in HAIX throughout the adsorption–desorption cycles, and that this effect is strongly promoted by the use of strong alkaline regeneration solution. This suggests that NPs in HAIX are not highly stable, and that the AIX resins, with this type of utilization, might not constitute a convenient support to such NPs (if oriented attachment is taking place). In general, more research needs to be performed to assess the long-term stability of HAIX, especially when repeatedly exposed to high pH values.

4.4. Challenges and limitations of HAIX adsorbents

Further work on tailoring of the two synthesis procedures is needed to achieve similar Fe loadings in the resins, obtaining a fairer P adsorption performances comparison. Also, all HAIX should be converted to either the chloride form or the sulphate form. This would provide further insights on the different synthesized NPs properties and P adsorption performances, leveling the influence of the resin counterion on adsorption selectivity. To better understand the adsorption–desorption mechanism in HAIX, further experiments such as pH and temperature-dependent adsorption (determining binding energies of P adsorbed onto AIX and onto NPs), isotopic exchange, and elemental measurements down to trace levels could provide valuable insights. Mössbauer spectroscopy revealed that the synthesized adsorbents, including the commercial HAIX Layne, consisted of goethite NPs, against what is claimed in previous studies, which reported generic amorphous HFO species. This stresses the importance of utilizing the proper tools to properly characterize samples. MS also revealed the NPs growth taking place in HAIX, via dissolution and reprecipitation and/or oriented attachment within the resin bead, mainly caused by the high alkaline conditions, questioning the stability of such ultrafine NPs and/or the robustness of AIX resins as a support. Furthermore, the desorption experiments highlighted the complex interaction between the OH^- regenerant molecules and the adsorbed P within the resin bead, resulting in inefficient desorption, questioning the suitability of HAIX for P recovery in applications at ultra-low concentrations. Hence, long term experiments with real wastewater and regeneration performed at pH 13–14 are needed, coupled with MS monitoring of the NPs, to fully assess the stability of such adsorbents, and in particular the potential of the Zn-doped iron oxide NPs. Nevertheless, these results strongly question the long-term stability end efficiency of HAIX for selective P recovery. Adsorption column experiments are highly recommended to better investigate and compare the applicability and long-term performances of these HAIX.

5. Conclusions

Previous studies showed Zn-doped iron (hydr)oxides NPs to be promising for improved P recovery and in this study they were for the first time successfully immobilized in an anion exchange resin and their performance compared to conventional Fe-based hybrid anion exchange adsorbents. The Zn-doped hybrid anion exchange adsorbents displayed on average similar to better P adsorption performances compared to the others, although further research is needed to confirm their potential.

Mössbauer spectroscopy revealed to be crucial to fully determine the nature and fate of the iron oxide nanoparticles in HAIX, showing that Fe-based HAIX contains goethite nanoparticles and not amorphous hydrous ferric oxides as previously claimed.

The adsorption tests confirmed the necessary role of the iron oxide nanoparticles for selective phosphate removal, highlighting the importance of performing adsorption at realistic water conditions.

Regeneration experiments confirmed that concentrated NaOH is able to fully regenerate HAIX (both the nanoparticles and the resin backbone), without the need of NaCl as claimed in literature. This allows to minimize the use of chemicals and to obtain a purer recovered phosphate stream, easier to treat. Moreover, these experiments revealed a complex interaction between OH^- and phosphate molecules within the resin backbone, never previously pointed out, resulting in an inefficient desorption at pH lower than 14. This highlighted an overconsumption of OH^- happening during phosphate desorption. This information is important for application, when considering chemical costs, and might help designing an appropriate and efficient desorption strategy (e.g., NaOH compensation).

Finally, Mössbauer spectroscopy revealed that HAIX regeneration with concentrated NaOH causes agglomeration and/or dissolution and re-precipitation of the nanoparticles within the resin backbone. This questions the stability of the NPs and/or the robustness of the AIX as a support for such NPs, especially in the long run, questioning the overall reusability of the adsorbent.

These findings will serve as a warning when interpreting adsorption and desorption mechanisms with HAIX, highlighting the importance of thoroughly understanding both mechanisms, and questioning the efficacy of AIX-based adsorbents for regenerative P adsorption at ultra-low concentrations.

Declaration of Competing Interest

The authors declare that they have no known competing financial interests or personal relationships that could have appeared to influence the work reported in this paper.

Data availability

Data will be made available on request.

Acknowledgments

This work was performed in the cooperation framework of Wetsus, European Centre of Excellence for Sustainable Water Technology (www.wetsus.nl). Wetsus is co-funded by the Dutch Ministry of Economic Affairs and Ministry of Infrastructure and Environment, the European Union Regional

Development Fund, the Province of Fryslân and the Northern Netherlands Provinces. This research received funding from the Netherlands Organization for Scientific Research (NWO) in the framework of the Innovation Fund for Chemistry, and from the Ministry of Economic Affairs and Climate Policy in the framework of the TKI/PPS-Toeslagregeling. The authors thank the participants of the research theme “Phosphate recovery” for the interest, fruitful discussions, and financial support. A special thanks goes to Raimonda Buliauskaitė (Aquacare) for the frequent knowledge exchange and interest in the research, Michel Steenvoorden and Maxim Ariens (TU Delft) for the support with Mössbauer spectroscopy related matters, Antony Cyril Arulrajan, Thomas Prot, Wokke Wijdeveld, Amanda Larasati, Sam Rutten, Daniele Chinello, Qingdian Shu (Wetsus) for the brainstorming sessions and insightful discussions, Gwendolina van der Linden for the work done together.

Appendix A. Supplementary data

Supplementary data to this article can be found online at https://doi.org/10.1016/j.cej.2023.145287.

References

[1] T. Möller, P. Sylvester, Effect of silica and pH on arsenic uptake by resin/iron oxide hybrid media, Water Res. 42 (2008) 1760–1766, https://doi.org/10.1016/j.watres.2007.10.044.

[2] S. Sarkar, A. Gupta, R.K. Biswas, A.K. Deb, J.E. Greenleaf, A.K. SenGupta, Well-head arsenic removal units in remote villages of Indian subcontinent: Field results and performance evaluation, Water Res. 39 (2005) 2196–2206, https://doi.org/10.1016/J.WATRES.2005.04.002.

[3] L. Cumbal, A.K. Sengupta, Arsenic removal using polymer-supported hydrated iron (III) oxide nanoparticles: Role of Donnan membrane effect, Environ. Sci. Tech. 39 (2005) 6508–6515, https://doi.org/10.1021/es050175e.

[4] M. German, H. Seingheng, A.K. SenGupta, Mitigating arsenic crisis in the developing world: Role of robust, reusable and selective hybrid anion exchanger (HAIX), Sci. Total Environ. 488–489 (2014) 547–553, https://doi.org/10.1016/j.scitotenv.2013.10.092.

[5] Q.J. Zhang, B.C. Pan, X.Q. Chen, W.M. Zhang, B.J. Pan, Q.X. Zhang, L. Lv, X. S. Zhao, Preparation of polymer-supported hydrated ferric oxide based on Donnan membrane effect and its application for arsenic removal, Sci. China, Ser. B 51 (2008) 379–385, https://doi.org/10.1007/s11426-007-0117-6.

[6] L.M. Blaney, S. Cinar, A.K. SenGupta, Hybrid anion exchanger for trace phosphate removal from water and wastewater, Water Res. 41 (2007) 1603–1613, https://doi.org/10.1016/j.watres.2007.01.008.

[7] D. Pinelli, S. Bovina, G. Rubertelli, A. Martinelli, S. Guida, A. Soares, D. Frascari, Regeneration and modelling of a phosphorous removal and recovery hybrid ion exchange resin after long term operation with municipal wastewater, Chemosphere 286 (2022), 131581, https://doi.org/10.1016/j.chemosphere.2021.131581.

[8] S. Guida, G. Rubertelli, B. Jefferson, A. Soares, Demonstration of ion exchange technology for phosphorus removal and recovery from municipal wastewater, Chem. Eng. J. 420 (2021), 129913, https://doi.org/10.1016/j.cej.2021.129913.

[9] A. Muhammad, A. Soares, B. Jefferson, The impact of background wastewater constituents on the selectivity and capacity of a hybrid ion exchange resin for phosphorus removal from wastewater, Chemosphere 224 (2019) 494–501, https://doi.org/10.1016/j.chemosphere.2019.01.085.

[10] P.S. Kumar, L. Korving, M.C.M. van Loosdrecht, G.J. Witkamp, Adsorption as a technology to achieve ultra-low concentrations of phosphate: Research gaps and economic analysis, Water Res. X. 4 (2019), 100029, https://doi.org/10.1016/J.WROA.2019.100029.

[11] X. Foster, C. Vaneeckhaute, Modifying the resin type of hybrid anion exchange nanotechnology (HAIX-Nano) to improve its regeneration and phosphate recovery efficiency, npj Clean Water 4 (2021) 1–8, https://doi.org/10.1038/s41545-021-00142-1.

[12] L. Carvalho, C. McDonald, C. de Hoyos, U. Mischke, G. Phillips, G. Borics, S. Poikane, B. Skjelbred, A.L. Solheim, J. Van Wichelen, A.C. Cardoso, M. Cadotte, Sustaining recreational quality of European lakes: minimizing the health risks from algal blooms through phosphorus control On secondment from CEH 2 to JRC 1, J. Appl. Ecol. 50 (2) (2013) 315–323.

[13] B.D. Martin, L. De Kock, M. Gallot, E. Guery, S. Stanowski, J. MacAdam, E. J. McAdam, S.A. Parsons, B. Jefferson, Quantifying the performance of a hybrid anion exchanger/adsorbent for phosphorus removal using mass spectrometry coupled with batch kinetic trials, Environ. Technol. (United Kingdom) 39 (2018) 2304–2314, https://doi.org/10.1080/09593330.2017.1354076.

[14] F.G. Donnan, Zeitschrift fuer Elektrochemie, Ang. Phys. Chem. 17 (1911) 572–581.

[15] F.G. Donnan, Theory of membrane equilibria and membrane potentials in the presence of non-dialysing electrolytes. A contribution to physical-chemical physiology, J. Memb. Sci. 100 (1995) 45–55, https://doi.org/10.1016/0376-7388(94)00297-C.

[16] S. Sarkar, A.K. Sengupta, P. Prakash, The Donnan membrane principle: Opportunities for sustainable engineered processes and materials, Environ. Sci. Tech. 44 (2010) 1161–1166, https://doi.org/10.1021/es9024029.

[17] D. Clifford, W.J. Weber, The determinants of divalent/monovalent selectivity in anion exchangers, React. Polym. 1 (1983) 77–89, https://doi.org/10.1016/0167-6989(83)90040-5.

[18] S. Subramonian, D. Clifford, Monovalent/divalent selectivity and the charge separation concept, React. Polym. Ion Exch. Sorbents. 9 (1988) 195–209, https://doi.org/10.1016/0167-6989(88)90033-5.

[19] Z. Hubicki, D. Koodynsk, Selective Removal of Heavy Metal Ions from Waters and Waste Waters Using Ion Exchange Methods, Ion Exch. Technol. (2012), https://doi.org/10.5772/51040.

[20] P. Suresh Kumar, W.W. Ejerssa, C.C. Wegener, L. Korving, A.I. Dugulan, H. Temmink, M.C.M. van Loosdrecht, G.-J. Witkamp, Understanding and improving the reusability of phosphate adsorbents for wastewater effluent polishing, Water Res. 145 (2018) 365–374.

[21] P. Suresh Kumar, T. Prot, L. Korving, K.J. Keesman, I. Dugulan, M.C.M. van Loosdrecht, G.J. Witkamp, Effect of pore size distribution on iron oxide coated granular activated carbons for phosphate adsorption – Importance of mesopores, Chem. Eng. J. 326 (2017) 231–239, https://doi.org/10.1016/j.cej.2017.05.147.

[22] P. Wilfert, P.S. Kumar, L. Korving, G.J. Witkamp, M.C.M. Van Loosdrecht, The Relevance of Phosphorus and Iron Chemistry to the Recovery of Phosphorus from Wastewater: A Review, Environ. Sci. Tech. 49 (2015) 9400–9414, https://doi.org/10.1021/acs.est.5b00150.

[23] R.M. Cornell, U. Schwertmann, The Iron Oxides (2003), https://doi.org/10.1002/3527602097.

[24] M. Kunaschk, V. Schmalz, N. Dietrich, T. Dittmar, E. Worch, Novel regeneration method for phosphate loaded granular ferric (hydr)oxide - A contribution to

phosphorus recycling, Water Res. 71 (2015) 219–226, https://doi.org/10.1016/j.watres.2015.01.001.
[25] S. Sarkar, P.K. Chatterjee, L.H. Cumbal, A.K. SenGupta, Hybrid ion exchanger supported nanocomposites: Sorption and sensing for environmental applications, Chem. Eng. J. 166 (2011) 923–931, https://doi.org/10.1016/j.cej.2010.11.075.
[26] S. Sarkar, L.M. Blaney, A. Gupta, D. Ghosh, A.K. SenGupta, Use of ArsenXnp, a hybrid anion exchanger, for arsenic removal in remote villages in the Indian subcontinent, React. Funct. Polym. 67 (2007) 1599–1611, https://doi.org/10.1016/j.reactfunctpolym.2007.07.047.
[27] K. Hristovski, P. Westerhoff, T. Möller, P. Sylvester, W. Condit, H. Mash, Simultaneous removal of perchlorate and arsenate by ion-exchange media modified with nanostructured iron (hydr)oxide, J. Hazard. Mater. 152 (2008) 397–406, https://doi.org/10.1016/j.jhazmat.2007.07.016.
[28] N.Y. Acelas, B.D. Martin, D. López, B. Jefferson, Selective removal of phosphate from wastewater using hydrated metal oxides dispersed within anionic exchange media, Chemosphere 119 (2015) 1353–1360, https://doi.org/10.1016/j.chemosphere.2014.02.024.
[29] K. Kalaitzidou, M. Mitrakas, C. Raptopoulou, A. Tolkou, P.A. Palasantza, A. Zouboulis, Pilot-Scale Phosphate Recovery from Secondary Wastewater Effluents, Environ. Process. 3 (2016) 5–22, https://doi.org/10.1007/s40710-016-0139-1.
[30] E. Kociołek-Balawejder, E. Stanisławska, I. Mucha, Freeze dried and thermally dried anion exchanger doped with iron(III) (hydr)oxide – Thermogravimetric studies, Thermochim Acta 680 (2019), 178359, https://doi.org/10.1016/j.tca.2019.178359.
[31] B.K. Mayer, D. Gerrity, B.E. Rittmann, D. Reisinger, S. Brandt-Williams, Innovative strategies to achieve low total phosphorus concentrations in high water flows, Crit. Rev. Environ. Sci. Technol. 43 (2013) 409–441, https://doi.org/10.1080/10643389.2011.604262.
[32] B. Pan, J. Wu, B. Pan, L.u. Lv, W. Zhang, L. Xiao, X. Wang, X. Tao, S. Zheng, Development of polymer-based nanosized hydrated ferric oxides (HFOs) for enhanced phosphate removal from waste effluents, Water Res. 43 (17) (2009) 4421–4429.
[33] Y. Zhang, X. She, X. Gao, C. Shan, B. Pan, Unexpected favorable role of Ca 2+ in phosphate removal by using nanosized ferric oxides confined in porous polystyrene beads, Environ. Sci. Tech. 53 (2019) 365–372, https://doi.org/10.1021/acs.est.8b05177.
[34] E. Murad, J. Cashion, Mössbauer Spectroscopy of Environmental Materials and Their Industrial Utilization, Springer US, Boston, MA, 2004.
[35] S. Sengupta, A. Pandit, Selective removal of phosphorus from wastewater combined with its recovery as a solid-phase fertilizer, Water Res. 45 (2011) 3318–3330, https://doi.org/10.1016/j.watres.2011.03.044.
[36] A. Sendrowski, T.H. Boyer, Phosphate removal from urine using hybrid anion exchange resin, Desalination 322 (2013) 104–112, https://doi.org/10.1016/j.desal.2013.05.014.
[37] P. Loganathan, S. Vigneswaran, J. Kandasamy, N.S. Bolan, Removal and recovery of phosphate from water using sorption, Crit. Rev. Environ. Sci. Technol. 44 (2014) 847–907, https://doi.org/10.1080/10643389.2012.741311.
[38] Y. Zhang, B. Pan, C. Shan, X. Gao, Enhanced Phosphate Removal by Nanosized Hydrated La(III) Oxide Confined in Cross-linked Polystyrene Networks, Environ. Sci. Tech. 50 (2016) 1447–1454, https://doi.org/10.1021/acs.est.5b04630.
[39] X. Huang, S. Guida, B. Jefferson, A. Soares, Economic evaluation of ion-exchange processes for nutrient removal and recovery from municipal wastewater, npj Clean Water 3 (2020), https://doi.org/10.1038/s41545-020-0054-x.
[40] K. Sivula, R. Van De Krol, Semiconducting materials for photoelectrochemical energy conversion, Nat. Rev. Mater. 1 (2016), https://doi.org/10.1038/natrevmats.2015.10.
[41] K. Zhang, J. Robinson, Doping of Two-Dimensional Semiconductors: A Rapid Review and Outlook, (2019). https://doi.org/10.1557/adv.2019.391.
[42] L.F. Liotta, M. Gruttadauria, G. Di Carlo, G. Perrini, V. Librando, Heterogeneous catalytic degradation of phenolic substrates: Catalysts activity, J. Hazard. Mater. 162 (2009) 588–606, https://doi.org/10.1016/j.jhazmat.2008.05.115.
[43] D.W. Lee, M.S. Lee, J.Y. Lee, S. Kim, H.J. Eom, D.J. Moon, K.Y. Lee, The review of Cr-free Fe-based catalysts for high-temperature water-gas shift reactions, Catal. Today 210 (2013) 2–9, https://doi.org/10.1016/j.cattod.2012.12.012.
[44] S. Rahim Pouran, A.A. Abdul Raman, W.M.A. Wan Daud, Review on the application of modified iron oxides as heterogeneous catalysts in Fenton reactions, J. Clean. Prod. 64 (2014) 24–35, https://doi.org/10.1016/j.jclepro.2013.09.013.
[45] S. Bram, M.N. Gordon, M.A. Carbonell, M. Pink, B.D. Stein, D.G. Morgan, D. Aguilà, G. Aromí, S.E. Skrabalak, Y. Losovyj, L.M. Bronstein, Zn2+ Ion Surface Enrichment in Doped Iron Oxide Nanoparticles Leads to Charge Carrier Density Enhancement, ACS Omega 3 (2018) 16328–16337, https://doi.org/10.1021/acsomega.8b02411.
[46] K. Govardhan, A. Nirmala Grace, Metal/metal oxide doped semiconductor based metal oxide gas sensors - A review, Sens. Lett. 14 (2016) 741–750, https://doi.org/10.1166/sl.2016.3710.
[47] H. Ito, S. Amagasa, N. Nishida, Y. Kobayashi, Y. Yamada, Wet chemical synthesis of zinc-iron oxide nanocomposite, Hyperfine Interact. 238 (2017) 1–5, https://doi.org/10.1007/s10751-017-1442-6.
[48] A. Lassoued, Synthesis and characterization of Zn-doped α-Fe2O3 nanoparticles with enhanced photocatalytic activities, J. Mol. Struct. 1239 (2021), 130489, https://doi.org/10.1016/j.molstruc.2021.130489.
[49] R. Medhi, C.H. Li, S.H. Lee, M.D. Marquez, A.J. Jacobson, T.C. Lee, T.R. Lee, Uniformly Spherical and Monodisperse Antimony- And Zinc-Doped Tin Oxide Nanoparticles for Optical and Electronic Applications, ACS Appl. Nano Mater. 2 (2019) 6554–6564, https://doi.org/10.1021/acsanm.9b01474.
[50] C.L. Warner, W. Chouyyok, K.E. Mackie, D. Neiner, L.V. Saraf, T.C. Droubay, M. G. Warner, R.S. Addleman, Manganese doping of magnetic iron oxide nanoparticles: Tailoring surface reactivity for a regenerable heavy metal sorbent, Langmuir 28 (2012) 3931–3937, https://doi.org/10.1021/la2042235.
[51] C. Belloni, L. Korving, G.-J. Witkamp, E. Brück, A.I. Dugulan, Effect of goethite doping using elements with different preferential oxidation states for improved reversible phosphate adsorption, J. Environ. Chem. Eng. 11 (2023), https://doi.org/10.1016/j.jece.2023.110505. Manuscript Submitted for Publication.
[52] C. Belloni, L. Korving, G.-J. Witkamp, E. Brück, A.I. Dugulan, Zn induced surface modification of stable goethite nanoparticles for improved regenerative phosphate adsorption, Manuscript Submitted for Publication, (2023).
[53] A.K. SenGupta, US7291578B2 Patent-protocol synthesis.pdf, (2007).
[54] Z. Klencsár, Mössbauer spectrum analysis by evolution algorithm, Nucl. Instruments Methods Phys. Res. Sect. B Beam Interact. Mater. Atoms. 129 (1997) 527–533, https://doi.org/10.1016/S0168-583X(97)00314-5.
[55] S. Lagergren, About the theory of so-called adsorption of soluble substances, K. Sven. Vetenskapsakademiens. 24 (2019) 1–39.
[56] S. Lagergren, Zur theorie der sogenannten adsorption gelöster stoffe, K. Sven. Vetenskapsakademiens. 24 (1898) 1–39.
[57] G. Blanchard, M. Maunaye, G. Martin, Removal of heavy metals from waters by means of natural zeolites, Water Res. 18 (1984) 1501–1507, https://doi.org/10.1016/0043-1354(84)90124-6.
[58] Q. Zhang, B. Pan, W. Zhang, B. Pan, Q. Zhang, H. Ren, Arsenate removal from aqueous media by nanosized Hydrated Ferric Oxide (HFO)-loaded polymeric sorbents: Effect of HFO loadings, Ind. Eng. Chem. Res. 47 (2008) 3957–3962, https://doi.org/10.1021/ie800275k.
[59] J. Zhang, Physical insights into kinetic models of adsorption, Sep. Purif. Technol. 229 (2019), 115832, https://doi.org/10.1016/j.seppur.2019.115832.
[60] S. Azizian, Kinetic models of sorption: A theoretical analysis, J. Colloid Interface Sci. 276 (2004) 47–52, https://doi.org/10.1016/j.jcis.2004.03.048.
[61] H.N. Tran, S.J. You, A. Hosseini-Bandegharaei, H.P. Chao, Mistakes and inconsistencies regarding adsorption of contaminants from aqueous solutions: A critical review, Water Res. 120 (2017) 88–116, https://doi.org/10.1016/j.watres.2017.04.014.
[62] T. Mubita, S. Porada, P. Aerts, A. van der Wal, Heterogeneous anion exchange membranes with nitrate selectivity and low electrical resistance, J. Memb. Sci. 607 (2020), 118000, https://doi.org/10.1016/j.memsci.2020.118000.
[63] R.M. Wheaton, W.C. Bauman, Properties of Strongly Basic Anion Exchange Resins, Ind. Eng. Chem. 43 (1951) 1088–1093, https://doi.org/10.1021/ie50497a027.
[64] R.W. Slingsby, C.A. Pohl, Anion-exchange selectivity in latex-based columns for ion chromatography, J. Chromatogr. A 458 (1988) 241–253, https://doi.org/10.1016/S0021-9673(00)90568-5.
[65] K.J. Powell, P.L. Brown, R.H. Byrne, T. Gajda, G. Hefter, S. Sjöberg, H. Wanner, Chemical speciation of environmentally significant heavy metals with inorganic ligands part 1: The Hg2+- Cl-, OH-, CO32-, so42-, and PO 43- aqueous systems (IUPAC technical report), Pure Appl. Chem. 77 (2005) 739–800, https://doi.org/10.1351/pac200577040739.
[66] C. Belloni, L. Korving, G.J. Witkamp, E. Brück, A.I. Dugulan, Effect of goethite doping using elements with different preferential oxidation states for improved reversible phosphate adsorption, J. Environ. Chem. Eng. 11 (5) (2023) 110505.
[67] Z. Fu, F. Wu, K. Song, Y. Lin, Y. Bai, Y. Zhu, J.P. Giesy, Competitive interaction between soil-derived humic acid and phosphate on goethite, Appl. Geochemistry. 36 (2013) 125–131, https://doi.org/10.1016/j.apgeochem.2013.05.015.
[68] M. Rashid, N.T. Price, M.Á. Gracia Pinilla, K.E. O'Shea, Effective removal of phosphate from aqueous solution using humic acid coated magnetite nanoparticles, Water Res. 123 (2017) 353–360, https://doi.org/10.1016/j.watres.2017.06.085.
[69] J. Antelo, F. Arce, M. Avena, S. Fiol, R. López, F. Macías, Adsorption of a soil humic acid at the surface of goethite and its competitive interaction with phosphate, Geoderma 138 (2007) 12–19, https://doi.org/10.1016/J.GEODERMA.2006.10.011.
[70] O.K. Borggaard, A.L. Gimsing, B.W. Strobel, Influence of humic substances on phosphate adsorption by aluminium and iron oxides, 127 (2005) 270–279. https://doi.org/10.1016/j.geoderma.2004.12.011.
[71] L. Weng, W.H. Van Riemsdijk, T. Hiemstra, Factors controlling phosphate interaction with iron oxides, J. Environ. Qual. 41 (2012) 628–635, https://doi.org/10.2134/jeq2011.0250.
[72] M.D.A. Bolland, A.M. Posner, J.P. Quirkk, Zinc adsorption by goethite in the absence and presence of phosphate, Aust. J. Soil Res. 15 (1977) 279–286, https://doi.org/10.1071/SR9770279.
[73] R.L. Penn, J.F. Banfield, Oriented attachment and growth, twinning, polytypism, and formation of metastable phases: Insights from nanocrystalline TiO2, Am. Mineral. 83 (1998) 1077–1082, https://doi.org/10.2138/am-1998-9-1016.
[74] R.L. Penn, J.F. Banfield, Imperfect oriented attachment: dislocation generation in defect-free nanocrystals, Science 281 (5379) (1998) 969–971.
[75] F. Huang, H. Zhang, J.F. Banfieldt, Two-stage crystal-growth kinetics observed during hydrothermal coarsening of nanocrystalline ZnS, Nano Lett. 3 (2003) 373–378, https://doi.org/10.1021/nl025836+.
[76] M.A. Anderson, M.I. Tejedor-Tejedor, R.R. Stanforth, Influence of Aggregation on the Uptake Kinetics of Phosphate by Goethite, Environ. Sci. Tech. 19 (1985) 632–637, https://doi.org/10.1021/es00137a009.
[77] J. Zhang, Z. Lin, Y. Lan, G. Ren, D. Chen, F. Huang, M. Hong, A multistep oriented attachment kinetics: Coarsening of ZnS nanoparticle in concentrated NaOH, J. Am. Chem. Soc. 128 (2006) 12981–12987, https://doi.org/10.1021/ja062572a.
[78] H. Yang, X. Zhou, T. Tang, X. Qi, C. Wang, J. Lan, Y. Wang, Y. Yang, G. Liu, Anisotropic growth of multi-twinned goethite particles by oriented aggregation, CrstEngComm 12 (2010) 4007–4011, https://doi.org/10.1039/c0ce00437e.